

On-site electron correlation nature of CrO₂ revealed by bulk sensitive soft-x-ray ARPES

F. Bisti^{1,†}, V. A. Rogalev¹, M. Karolak², S. Paul³, A. Gupta³, T. Schmitt¹, G. Güntherodt⁴, G. Sangiovanni², G. Profeta⁵ and V. N. Strocov¹

¹*Swiss Light Source, Paul Scherrer Institute, CH-5232 Villigen PSI, Switzerland*

²*Institut für Theoretische Physik und Astrophysik, Universität Würzburg, Germany*

³*MINT Center, University of Alabama, Tuscaloosa, Alabama 35487, USA*

⁴*II. Physikalisches Institut, RWTH Aachen University, 52074 Aachen, Germany*

⁵*Dipartimento di Scienze Fisiche e Chimiche, Università dell'Aquila, Via Vetoio 10, 67100, L'Aquila, Italy*

[†]*Present address: ALBA Synchrotron Light Facility, 08290 Cerdanyola del Vallès, Spain (email: fbisti@cells.es).*

Abstract

Chromium dioxide CrO₂ belongs to a class of materials called half-metals, whose peculiar aspect is to act as a metal in one spin orientation and as semiconductor or insulator in the opposite one. Despite numerous experimental and theoretical studies motivated by technologically important applications of this material in spintronics and high-capacity data storage, its fundamental properties such as momentum resolved electron dispersions and

Fermi surface have so far remained experimentally inaccessible due to metastability of its surface that instantly reduces to amorphous Cr_2O_3 . In this work we demonstrate that direct access to the native electronic structure of CrO_2 can be achieved with soft-X-ray angle-resolved photoemission spectroscopy whose large probing depth allows penetration through the Cr_2O_3 layer. For the first time the electronic dispersions and Fermi surface of CrO_2 are measured which are fundamental requisites to solve the long debate on the nature of electronic correlations in this material. Since density functional theory augmented by a weak local Coulomb repulsion gives an exhaustive description of our spectroscopic data, we rule out strong-coupling theories of CrO_2 . Crucial for correct interpretation of our experimental data in terms of the valence band dispersions is a non-trivial spectral response of CrO_2 caused by interference effects in the photoemission process originating from the non-symmorphic space group of the rutile crystal structure of CrO_2 .

Introduction

In the group of the mostly antiferromagnetic insulating 3d transition-metal oxides, chromium dioxide (CrO_2) is the only one possessing a ferromagnetic conducting phase. Its ground-state Fermi surface (FS) is composed of 100% spin polarized electrons, resulting in so-called “half-metallic” nature of CrO_2 . Since almost 30 years, the half-metallicity has been correctly predicted within the simple density functional theory (DFT) using the local spin-density approximation (LSDA) of the ground-state electron exchange-correlation [1]. A clear experimental demonstration was obtained by point contact Andreev reflection, showing a spin polarization of the conductive electrons higher than 90% [2] and later in subsequent studies higher than 98% [3]. The half-metallicity of CrO_2 finds important practical application in spintronics and data storage. Furthermore, it was demonstrated the exciting possibility to

inject spin-triplet supercurrent into CrO_2 [4] which sets up interesting connections between spintronics and superconductivity. However, one of the biggest limitations to fully exploit the device potential of the half-metallicity of CrO_2 is its dramatic deterioration with temperature, which is therefore considered as a property restricted to the ground state. Several depolarization mechanisms have been suggested [5, 6], including those where electronic correlations might play an important role [6, 7].

The electron correlation effects in CrO_2 beyond the mean-field approach within the local density approximation are still under debate, because the experimental data reported so far diverge concerning the degree of their contribution. In the DFT-LSDA framework, the calculated density of states (DOS) does not reproduce the angle-integrated photoemission spectra of the valence band [8, 9, 10]. However, a better agreement can be obtained with introduction of an on-site Coulomb correlation term within the LSDA+ U approach using theoretically derived values of 3 eV and 0.87 eV for U and J , respectively [11]. On the other hand, optical conductivity [12] and magnetic anisotropy [13] are better modelled by just static LSDA, and magneto-optical Kerr spectroscopy data required only the gradient corrections within the generalized gradient approximation (GGA) of the static exchange-correlation [14]. The problem has also been the subject of dynamic mean field theory based calculations, including dynamic electron exchange-correlation, in combination with DFT (LSDA+DMFT). In ref. [15], the authors claimed an improved quantitative agreement in the interpretation of photoemission data with LSDA+DMFT ($U=5$ eV and $J=1$ eV) as compared to LSDA or LSDA+ U as well as semi-quantitative agreement with thermodynamic and direct current transport measurements. A further LSDA+DMFT work [7] reduced the Coulomb and Hund's terms to $U=3$ eV and $J=0.9$ eV, respectively, and demonstrated the appearance of non-quasiparticle states in the minority spin channel near the Fermi level E_F . The presence

of these non-quasiparticles was claimed to be essential for correct quantitative description of the spin polarization temperature dependence [7]. These results emphasize the fact that a correct treatment of the electron correlations in CrO_2 is not just a pure theoretical issue but has important implications for its exotic transport properties. Different scenarios for the transport phenomena were suggested, depending on how the correlations are modelled [7, 12, 16]. However, a complete understanding of the nature of electron correlations in CrO_2 requires momentum-resolved experimental data on the electronic structure of this material.

Angle-resolved photoemission spectroscopy (ARPES) represents a natural experimental technique to directly probe the momentum resolved electronic structure. However, the conventional ARPES in the photon energy range 20-200 eV has a very small probing depth as characterized by photoelectron mean free path much below 1 nm. This technique is therefore inapplicable to CrO_2 because its surface is metastable at normal conditions and, immediately after the synthesis, develops an amorphous insulating film of antiferromagnetic Cr_2O_3 with a thickness of roughly 2 nm [17] well above the conventional ARPES probing depth. On the other hand, it has been demonstrated that the use of photons with higher energies towards 1200 eV [10] or lower energies towards 8 eV [18] deliver a probing depth around 2 nm, which allows detection of photoelectrons emitted from CrO_2 through the Cr_2O_3 overlayer.

In this work, we demonstrate that the momentum-resolved electron dispersions and FS of CrO_2 can be explored by bulk sensitive soft-x-ray ARPES (SX-ARPES) using photon energies in the range of 320-820 eV. Moreover, the increase of the photoelectron mean free path in this energy range reduces, by the Heisenberg relation, the intrinsic uncertainty of the surface-perpendicular momentum k_z [19], allowing an accurate mapping of the 3D electron dispersions. We find that the experimental FS appears composed mainly of an

electron pocket around the Γ point and a hole pocket around the Z point of the tetragonal Brillouin zone. Our first-principles DFT calculations, taking into account exotic matrix element effects in the ARPES response of CrO_2 originating from its non-symmorphic rutile space group, demonstrate that the LSDA + U approximation with the on-site U_{eff} parameter ($U_{\text{eff}} = U - J$) equal to 1 eV (0.4 eV with the use of GGA) deliver an accurate description of the CrO_2 band structure. We conclude therefore that CrO_2 can be considered as a moderately correlated material with the electron correlations effects essentially exhausted by the local on-site correlations.

Results

Fermi surface and photoemission interference effects

In Fig. 1 we gather our theoretical and experimental information on the FS of CrO_2 . The FS obtained from our LSDA+ U calculations with $U_{\text{eff}} = 1$ eV (for the determination of U_{eff} see below) is reported in Fig. 1(a) inscribed into the first Brillouin zone (BZ). The theoretical FS is fully spin polarized and characterized by a quasi-isotropic electron pocket around the Γ point (violet surface), a hole pocket along the Γ -Z direction (yellow) that barely closes near the Z points, and another electron pocket around the A point (violet). Different colored planes $p1$ - $p4$ in Fig. 1(a) show the FS cuts explored in our SX-ARPES experiment, the surface-parallel cut $p1$ under sample rotation and the surface-perpendicular cuts $p2$ - $p4$ under variation of photon energy. The top maps in the respective panels $p1$ - $p4$ report the corresponding ARPES intensity rendered into the electron momentum coordinates k_x, k_y and k_z corrected for the incident X-ray photon momentum. The sharpness of the FS contours in the k_z direction confirms sharp definition of k_z resulting from the photoelectron mean free

path increase in the SX-ARPES energy range [19].

The bottom maps in the $p1$ - $p4$ panels in Fig. 1 report the same experimental data overlaid with the LSDA+ U calculated FS contours. The contours shown on the $k_{x,y}>0$ side of these maps (marked "2-Cr BZ") correspond to the full rutile unit cell of CrO_2 including two Cr atoms, and the ones on the $k_{x,y}<0$ side (marked "1-Cr BZ") unfold these contours onto a reduced body-centered tetragonal unit cell including one Cr atoms (see below). The most striking feature of our data in comparison with the full unit cell calculations is particularly evident in the $p2$ cut: the electron pocket around Γ (violet contours) is experimentally present only in every second BZ, centred at the surface-perpendicular momenta k_z equal to even integers n of $2\pi/a$ (in our case $n = 8$ and 10), and disappears in those centred at odd integers ($n = 7$ and 9 designated as Γ'). Complementarily, in the next BZ along the surface-parallel momentum k_x represented in the cut $p3$, the electron pockets are visible at k_z equal to the odd integers of $2\pi/a$ but disappear at even ones. Furthermore, in the $p2$ cut we distinguish also the hole pockets (yellow contours) which show the same odd-even alternation. In this way, our data exhibits a periodicity in reciprocal space larger than expected, meaning that in the real space this periodicity should be related to an effective unit cell smaller than the formal one. Similar mismatch between the real space periodicity and that obtained in ARPES spectra has recently observed in iron pnictides [20, 21, 22] as well as in a series of materials whose crystal structure possesses non-symmorphic space group such as graphite [23], BiTeCl [24] and decagonal Al-Ni-Co quasicrystal [25].

In the case of CrO_2 , the apparent twice large period of the ARPES response in \mathbf{k} -space also originates from non-symmorphicity of its rutile-type space group (D_{4h}^{14} : $P4_2/mnm$). The Cr atoms adopt the body-centered tetragonal lattice surrounded by distorted octahedron of oxygen atoms (see Fig. 1b). The octahedron in the center is rotated by 90° along the c -axis

with respect to the ones at the corners. The presence of this screw axis reduces the accessible final states in the photoemission process belonging to different irreducible representations along the high symmetry lines, which appears as alternating visibility of the spectral features through the successive BZs [23, 26]. This effect can be theoretically described based on formal unfolding of band structure from the full to an effective unit cell, as has recently been demonstrated for iron pnictides [20]. Briefly, this procedure is based on projection of the Bloch wavefunctions of the non-symmorphic crystal to eigenfunctions in the corresponding symmorphic structure (that obeys, apart from the lattice translations, to all symmetry operations leaving one common point fixed) and to the additional symmetry operation of the non-symmorphic space group. In our case, the right linear combination to describe the Cr-derived d -states near E_F is composed of the d_{xy} , d_{yz-zx} and d_{yz+zx} atomic orbitals of the two different Cr atoms in their local coordinate frame with respect to the oxygen octahedron (for further details see Methods). In practice, the unfolding procedure assigns to the first-principles eigenvalues weights proportional to the projections of the corresponding eigenfunctions onto the new basis set. The results of this procedure performed with our LSDA+ U calculations are reported in the bottom maps of Fig. 1 on their left ($k_{x,y} < 0$) side marked "1-Cr BZ". The unfolding perfectly reproduces the experimental odd-even visibility of the electron pockets around the Γ and Γ' points in $p1$ - $p2$ as well as the hole pockets around the Z point in $p1$.

Having understood this crucial aspect of the ARPES response of CrO_2 , we will discuss other FS cuts in Fig. 1. Due to the unit cell symmetry between the k_y and k_z directions, the (k_x, k_y) cut in the panel $p1$ is identical to the (k_x, k_z) one in the panel $p2$, although the latter shows the FS contours clearly affected by the intrinsic k_z broadening [19]. Furthermore, the $p4$ panel clearly reveals the small electron pocket around the A point in perfect agreement

with the LSDA+ U predictions, Fig. 1 (a).

Sharp contrast and excellent statistics of our SX-ARPES data confirm that this technique is indeed capable of digging out the electronic structure of CrO₂ through the Cr₂O₃ overlayer. The experiment reveals the FS topology as composed of two electron pockets around the Γ and A points and one hole pocket between the Γ and Z points, Fig. 1(a). Taking into account the matrix element effects, the experimental results are fully consistent with our LSDA+ U calculations where all Fermi states belong to the majority spin channel and have the d_{yz-zx} and d_{yz+zx} character. The agreement extends on both topology and Luttinger volume of the FS pockets.

Band dispersions

Further information about the electronic structure of CrO₂ is contained in the experimental band dispersions along the Γ -X and Γ -Z directions reported in Fig. 2. Each row of the panels *a-d*, from left to right, first shows the raw ARPES image. On top of the dispersive coherent spectral component, each image contains a large non-dispersive component which can be modelled by angle integration of the raw images, as shown in the next panel. This component is formed, first, by photoexcitation in the amorphous Cr₂O₃ overlayer and, second, by photoelectrons excited in CrO₂ and quasielastically scattered in Cr₂O₃ on their escape to vacuum and thus reflecting the \mathbf{k} -integrated DOS of CrO₂. We note however that experimental non-dispersive component is predominated by photoexcitation in amorphous Cr₂O₃ because it strongly deviates from the expected DOS of CrO₂ in Fig. 3 (a). This fact calls for re-consideration of the previous works where the value of U_{eff} was estimated by comparison with angle-integrated spectra. The coherent component characteristic of the crystalline CrO₂ is obtained by subtracting of the non-dispersive component from the raw

images (see ‘Data Processing’ in the ‘Methods’) as shown in the next panels. These images reveal sharp band dispersions, allowing direct comparison with our LSDA+ U calculations on the rightmost panels. Overlaid on the same experimental data, the unfolded theoretical bands presented on the $k_x < 0$ side (marked "1-Cr BZ") again truly reproduce the matrix element effects in our data in comparison with the ones without unfolding shown on the $k_x > 0$ side (marked "2-Cr BZ"). In particular, the calculation along the Γ -X direction correctly reproduces the d_{yz+zx} -like band forming the central FS pocket around the Γ point (although slightly overestimates its size) and the unfolding reproduces the cancellation of this band in the second BZ. The same striking agreement between the experiment and unfolded calculated bands is found along the Γ -Z direction (except the deep oxygen-derived sp -states which are not correctly described by the d -orbitals of our unfolding basis set).

The dispersions along the Γ -Z direction are most sensitive to variations of U_{eff} in our LSDA+ U calculations (see below) and were therefore carefully investigated using different photon energies and polarizations of incident X-rays. A zoom-in of the near- E_F region measured at 603 eV ($k_z = 9 \cdot 2\pi/a$) is reported in Fig. 2 (c) and linear dichroism at 748 eV ($k_z = 10 \cdot 2\pi/a$) in (d,e). Switching between the s - and p -polarization switches the ARPES response between different sets of bands. The same linear dichroism has been noted in ARPES experiments on TiO_2 and interpreted as switching from Γ to the next Γ' point [26]. We note that the band calculations without unfolding ("2-Cr BZ") demonstrate the absence of hybridization between different bands in their intersections at the X and Z points (in particular, in the cone at the Z point near E_F). This effect appears because the two intersecting bands belong to different irreducible representation of the non-symmorphic space group $D_{4h}^{14}:\text{P4}_2/\text{mnm}$ of CrO_2 . Naturally, in the unfolded band representation ("1-Cr BZ") the weight of one of the two branches vanishes.

Determination of the static effective Coulomb interaction

The effect of the on-site Hubbard-like parameter U_{eff} on the majority spin band structure calculated within the LSDA+ U scheme is reported in Fig. 3(b). Higher U_{eff} values push the d_{xy} band to higher binding energy (most visible along the Γ -Z direction, as noted before, in the interval from -0.6 to -1.1 eV) and, at the same time, push the d_{yz+zx} band closer to E_F . The most satisfactory match between the LSDA+ U calculated and experimental data (grey points obtained by fitting of the spectral peaks) is achieved as the best compromise between these two trends reached with $U_{\text{eff}} = 1$ eV. Furthermore, in Fig. 3(b) we also report the calculations using the GGA for the static exchange-correlation (PBE). The same good agreement with the experiment is achieved, but in this case with smaller $U_{\text{eff}} = 0.4$ eV (the difference is attributed mainly to higher accuracy of the equilibrium lattice constant in GGA than in LDA [27]). The effect of U_{eff} on the FS contours is reported in Fig. 3(c). Their modifications with U_{eff} are essentially restricted by the neighborhood of the Z and A points due to the fact that the on-site correlations effects do not much affect energies of the d_{yz+zx} and d_{yz-zx} orbitals.

Discussion

Excellent agreement of our LSDA+ U_{eff} calculations with relatively small value of U_{eff} (especially for the GGA exchange-correlation) evidences that CrO_2 is a moderately correlated material where the electron correlations are essentially exhausted by the local on-site correlations described by U_{eff} as a combination of the Coulomb interaction parameter U and the Hund's spin coupling parameter J .

The picture of moderate electron correlations in CrO_2 has important implications for

the debated mechanism of its depolarization at higher temperature [5, 6]. Indeed, this picture allows us to conjecture that the depolarization appears due to one-electron mechanisms such as formation of sublattices with different spins or phonon interactions, rather than strong electron correlation effects such as non-quasiparticle states or orbital Kondo interaction [5, 6, 7]. Furthermore, the relevance of the DFT+ U framework of the electron correlation poses solid basis for realization of new theoretically predicted electronic phases in CrO_2 thin films. Such phases can include, in particular, a half-semimetallic Dirac cone formed in a thin film or heterostructure consisting of a few CrO_2 layers interfaced with TiO_2 [28] or an emergent topological superconductor with a single chiral Majorana edge state formed by two atomic layer of CrO_2 interfaced with a superconductor [29].

We want to note that we have also performed calculations beyond the static DFT+ U approximation to the Coulomb interaction. We calculated the k -resolved spectral function in the framework of the DFT+DMFT scheme using a t_2g -only model. However, despite a variation of the interaction parameters the agreement of these preliminary DMFT spectra with our SX-ARPES data was inferior compared to the simple LSDA+ U . The investigation into the reasons for this is ongoing and a full account will be given elsewhere [30].

As the final remark, we stress that the crucial element of our exhaustive picture of electronic structure of the paradigm half-metal CrO_2 has been the use of SX-ARPES providing large probing depth and sharp definition of three-dimensional electron momentum. The non-trivial interference effects in the ARPES response of CrO_2 caused by its non-symmorphic space group were described by band structure unfolding onto an effective smaller unit cell using atomic projections. Deciphered with the unfolding, our experimental dataset yields the most exhaustive momentum-resolved description of the electron dispersions and FS so

far achieved for CrO₂. We establish its FS topology as composed of two electron pockets around the Γ and A point and a hole pocket along the Γ -Z direction. At least at low temperature, our theoretical description finds full spin polarization of the Fermi states confirming the half-metallic nature of CrO₂. The subsequent knowledge of the orbital character of the bands reveals the itinerant ferromagnetic phase of CrO₂ composed by the d_{yz+zx} and d_{yz-zx} orbitals, and the localized d_{xy} orbital.

Methods

Samples and SX-ARPES measurements

Epitaxial thin films of CrO₂ (100) were grown by chemical vapor deposition in oxygen atmosphere on top of a TiO₂(100) substrate [31] at the MINT Center, University of Alabama, USA. The SX-ARPES experiments at different polarizations of incident X-rays were performed at the SX-ARPES endstation [32] of the ADRESS beamline [33] at the Swiss Light Source synchrotron facility, Villigen-PSI, Switzerland. The samples were transferred for SX-ARPES measurements ex-situ without any treatment. The sample temperature during the measurements was around 12 K to quench suppression of the coherent spectral weight due to thermal effects [34]. The combined (beamline and analyzer) energy resolution was set to vary between 40 and 100 meV through the incident photon energy range 300-900 eV. The sample surface was oriented normal to the analyzer axis, and the grazing incidence angle of photons was 20°. Details of the experimental geometry as well as photon momentum corrected transformation of the emission angles and energies into \mathbf{k} values can be found in [32].

Data processing

The experimental FS maps in Fig. 1 were obtained by the integration of the spectral intensity within ± 0.05 eV around E_F . To compensate the photoexcitation cross-section variation over the large photon energy range of panels $p2$, $p3$ and $p4$, we normalized the maps to the same integral intensity over 90% of their angular range. The non-dispersive spectral component in Fig. 2 was evaluated by angle integration corrected for angle dependent transmission of the ARPES analyzer.

Theoretical calculations and unfolding procedure

The DFT calculations on CrO_2 were performed using the Vienna Ab-initio Simulation Package (VASP) [35] with a plane-wave cutoff of 350 eV and $6 \times 6 \times 9$ Monkhorst-Pack grid sampling for the charge-density integration. The LDA and the GGA-PBE exchange-correlation functionals were used. In both cases, the on-site Coulomb correlation (U_{eff}) was tuned to obtain the best agreement with the experimental data, focusing on the most sensitive Γ -Z direction. We adopted the experimental lattice parameters $a=b= 4.421$ Å and $c=2.917$ Å [36].

The unfolding procedure is obtain by the projections on the basis set $\{\varphi_{(S)}^i\}$ ($i=xy, yz-zx, yz+zx$) formed by the d_{xy} , d_{yz-zx} and d_{yz+zx} atomic orbitals for the two different Cr sites in their local coordinate frame ($S=\text{Cr1}, \text{Cr2}$). This set of orbitals is sufficient for the d -states in vicinity of E_F away from the oxygen derived sp -states deeper in the valence band. The partial spectral weight from the i -type d atomic orbital associated to the eigenstate $\varepsilon_{n,k}$ of the eigenfunction $\psi_{n,k}$ is calculated as $W_{n,k}^i = \left| \sum_S e^{ikR_S} \langle \varphi_{(S)}^i | \psi_{n,k} \rangle \right|^2$, (R_S is the position vector of S atom) and the total spectral weight is the sum of these three single contributions

$W_{n,k}^{tot} = \sum_i W_{n,k}^i$. The unfolded band structure is represented with the point size proportional to the total spectral weight, while its color is obtained from the percentage representation of colors in the RGB format (red, green and blue) proportional to $W_{n,k}^{yz+zx}$, $W_{n,k}^{yz-zx}$ and $W_{n,k}^{xy}$ respectively.

Acknowledgements

We thank H. Dil, J. Minar, Yu. S. Dedkov and O. Gunnarsson for promoting discussions. The research leading to these results has received funding from the Swiss National Science Foundation under the grant agreement n.° 200021_146890 and European Community's Seventh Framework Programme (FP7/2007-2013) under the grant agreement n.°290605 (PSI-FELLOW/COFUND).

References

- [1] Schwarz, K. CrO₂ predicted as half metallic ferromagnet. *J. Phys. F : Met. Phys.* **16**, L211-L215 (1986).
- [2] Soulen, Jr R. J. *et al.* Measuring the Spin Polarization of a Metal with a Superconducting Point Contact. *Science* **282**, 85-88 (1998).
- [3] Anguelouch, A. *et al.* Near-complete spin polarization in atomically-smooth chromium-dioxide epitaxial films prepared using a CVD liquid precursor. *Phys. Rev. B* **64**, 180408(R) (2001).
- [4] Keizer, R. S. *et al.* A spin triplet supercurrent through the half-metallic ferromagnet CrO₂. *Nature* **439**, 825-827 (2006).
- [5] Skomski, R. Finite-temperature depolarization in half metals. *J. Phys.: Condens. Matter*

19, 315202 (2007).

[6] Katsnelson, M. I., Irkhin, V. Yu., Chioncel, L., Lichtenstein, A. I., de Groot, R. A. *Rev. Mod. Phys.* **80**, 315-378 (2008).

[7] Chioncel, L. *et al.* Half-metallic ferromagnetism and spin polarization in CrO₂. *Phys. Rev. B* **75**, 140406(R) (2007).

[8] Tsujioka, T. *et al.* Hubbard splitting and electron correlation in the ferromagnetic metal CrO₂. *Phys. Rev. B* **56**, R15509-R15512 (1997).

[9] Chang, C. F. *et al.* Electronic structure of CrO₂ studied by magnetic circular dichroism in resonant photoemission. *Phys. Rev. B* **71**, 052407 (2005).

[10] Sperlich, M. *et al.* Intrinsic correlated electronic structure of CrO₂ revealed by hard x-ray photoemission spectroscopy. *Phys. Rev. B* **87**, 235128 (2013).

[11] Korotin, M. A., Anisimov, V. I., Khomskii, D. I. & Sawatzky, G. A. CrO₂: A Self-Doped Double Exchange Ferromagnet. *Phys. Rev. Lett.* **80**, 4305-4308 (1998).

[12] Mazin, I. I., Singh, D. J. & Ambrosch-Draxl, C. Transport, optical, and electronic properties of the half-metal CrO₂. *Phys. Rev. B* **59**, 411-418 (1999).

[13] Toropova, A., Kotliar, G., Savrasov, S. Y. & Oudovenko, V. S. Electronic structure and magnetic anisotropy of CrO₂. *Phys. Rev. B* **71**, 172403 (2005).

[14] Kuneš, J. *et al.* Electronic structure of CrO₂ as deduced from its magneto-optical Kerr spectra. *Phys. Rev. B* **65**, 165105 (2002).

[15] Craco, L., Laad, M. S. & Müller-Hartmann, E. Orbital Kondo Effect in CrO₂: A Combined Local-Spin-Density-Approximation Dynamical-Mean-Field-Theory Study. *Phys. Rev. Lett.* **90**, 237203 (2003).

[16] Brener, N. E. *et al.* Electronic structure and Fermi surface of CrO₂. *Phys. Rev. B* **61**, 16582-16588 (2000).

- [17] Leo, T. *et al.*, Sign of tunneling magnetoresistance in CrO₂-based magnetic tunnel junctions. *Appl. Phys. Lett.* **91**, 252506 (2007).
- [18] Fujiwara, H. *et al.* Intrinsic spin polarized electronic structure of CrO₂ epitaxial film revealed by bulk-sensitive spin-resolved photoemission spectroscopy. *Appl. Phys. Lett.* **106**, 202404 (2015).
- [19] Stroscov, V. N. Intrinsic accuracy in 3-dimensional photoemission band mapping. *J. Electron Spectrosc. Relat. Phenom.* **130**, 65-78 (2003).
- [20] Tomić, M., Jeschke, H. O. & Valentí, R. Unfolding of electronic structure through induced representations of space groups : Application to Fe-based superconductors. *Phys. Rev. B* **90**, 195121 (2014).
- [21] Moreschini, L. *et al.* Consequences of Broken Translational Symmetry in FeSe_xTe_{1-x}. *Phys. Rev. Lett.* **112**, 087602 (2014).
- [22] Lin, C.-H. *et al.* One-Fe versus Two-Fe Brillouin Zone of Fe-Based Superconductors: Creation of the Electron Pockets by Translational Symmetry Breaking. *Phys. Rev. Lett.* **107**, 257001 (2011).
- [23] Pescia, D., Law, A. R., Johnson, M. T. & Hughes, H. P. Determination of observable conduction band symmetry in angle-resolved electron spectroscopies: non-symmorphic space groups. *Solid State Commun.* **56**, 809-812 (1985).
- [24] Landolt, G. *et al.* Bulk and surface Rashba splitting in single termination BiTeCl. *New J. Phys.* **15**, 085022 (2013).
- [25] Rogalev, V. A. *et al.* Fermi states and anisotropy of Brillouin zone scattering in the decagonal Al-Ni-Co quasicrystal. *Nat. Commun.* **6**, 8607 (2015).
- [26] Hardman, P. J. *et al.* Valence-band structure of TiO₂ along the Γ - Δ -X and Γ - Σ -M directions. *Phys. Rev. B* **49**, 7170 (1994).

- [27] Sims, H., Oset, S. J., Butler, W. H., MacLaren, J. M. & Marsman, M. Determining the anisotropic exchange coupling of CrO₂ via first-principles density functional theory calculations. *Phys. Rev. B* **81**, 224436 (2010).
- [28] Cai, T. *et al.* Single-Spin Dirac Fermion and Chern Insulator Based on Simple Oxides. *Nano Lett.* **15**, 6434–6439 (2015).
- [29] Chung, S. B., Zhang, H.-J., Qi, X.-L. & Zhang, S.-C. Topological superconducting phase and Majorana fermions in half-metal/superconductor heterostructures. *Phys. Rev. B* **84**, 060510(R) (2011).
- [30] Karolak, M. *et al.* To be published.
- [31] Miao, G., Xiao & G., Gupta, A. Variations in the magnetic anisotropy properties of epitaxial CrO₂ films as a function of thickness. *Phys. Rev. B* **71**, 094418 (2005).
- [32] Strocov, V. N. *et al.* Soft-X-ray ARPES facility at the ADRESS beamline of the SLS: Concepts, technical realisation and scientific applications. *J. Synchrotron Rad.* **21**, 32-44 (2014).
- [33] Strocov, V. N. *et al.* High-resolution soft X-ray beamline ADRESS at the Swiss Light Source for resonant inelastic X-ray scattering and angle-resolved photoelectron spectroscopies. *J. Synchrotron Rad.* **17**, 631 (2010).
- [34] Braun, J. *et al.* Exploring the XPS limit in soft and hard x-ray angle-resolved photoemission using a temperature-dependent one-step theory. *Phys. Rev. B* **88**, 205409 (2013).
- [35] Kresse, G. & Furthmüller, J. Efficient iterative schemes for ab initio total-energy calculations using a plane-wave basis set. *Phys. Rev. B* **54**, 11169 (1996).
- [36] Cloud, W. H., Schreiber, D. S. & Babcock, K. R. XRay and Magnetic Studies of CrO₂ Single Crystals. *J. Appl. Phys.* **33**, 1193 (1962).

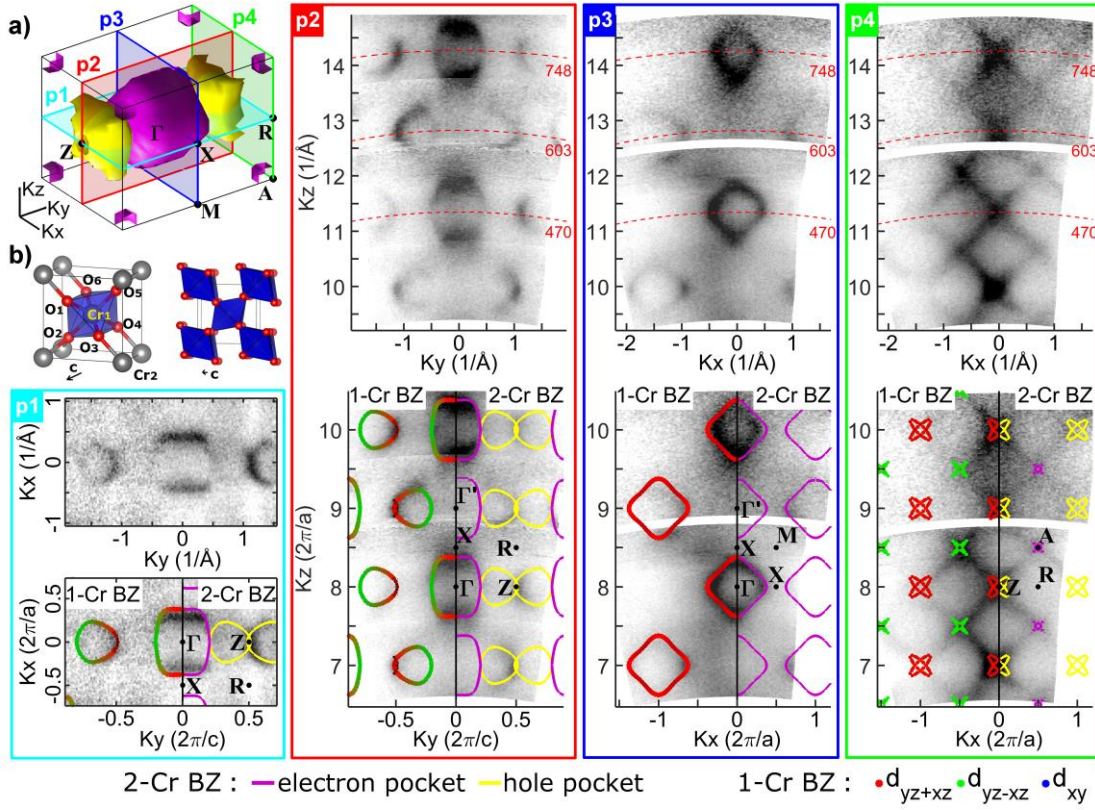


Fig. 1. Experimental and theoretical FS of CrO₂: (a) LSDA+*U* ($U_{\text{eff}}=1\text{eV}$) calculations; (b) Unit cell of CrO₂; (p1-p4, maps at *top*) Experimental ARPES maps of the FS along the planes marked at (a); (p1-p4, maps at *bottom*) the same data overlaid with the LSDA+*U* ($U_{\text{eff}}=1\text{eV}$) results on the right ($k_{x,y}>0$) side. The apparent doubling of the FS periodicity in \mathbf{k} -space is due to the non-symmorphic space group of CrO₂. This is confirmed by unfolding of the calculated FS onto the 1-Cr cell shown on the left ($k_{x,y}<0$) side. These ARPES data were collected with *p*-polarized light at photon energy of 470 eV for p1 and varied in the 320-820 eV range for (p2-p4) as indicated at the top panels.

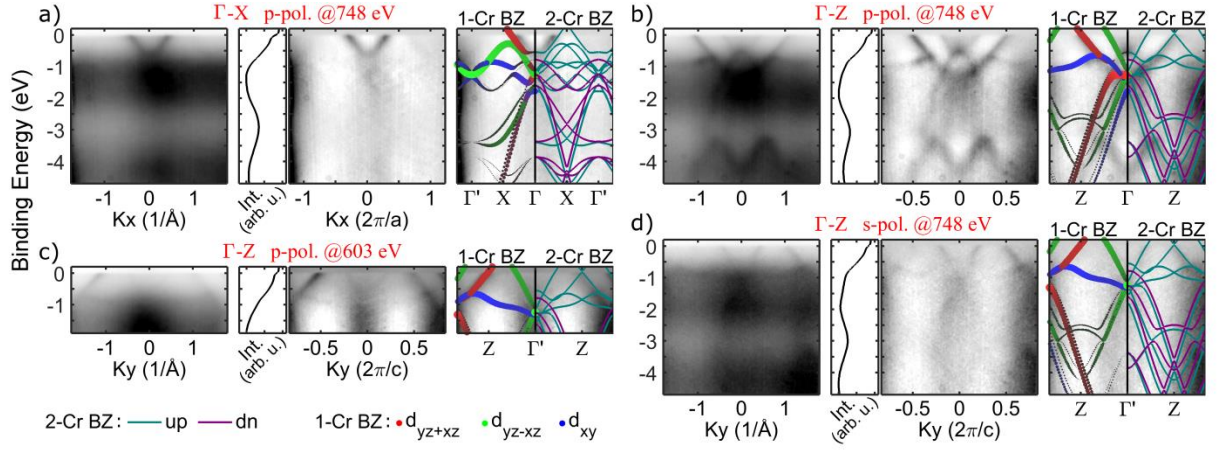


Fig. 2: Experimental and theoretical band dispersions in CrO_2 along the Γ -X and Γ -Z directions. The photon energy and X-ray polarization are indicated on top of each row *a-d* of the panels representing, from left to right: the row ARPES image; non-dispersive spectral component coming mostly from the Cr_2O_3 overlayer; dispersive spectral component from CrO_2 ; the same data on the $k_{x,y}>0$ side overlaid with the LSDA+ U ($U_{\text{eff}} = 1\text{eV}$) dispersions (majority spins in cyan and minority in magenta) and on the $k_{x,y}<0$ side with the corresponding bands unfolded onto the in 1-Cr BZ. The unfolding well reproduces the experimental intensity variation through the successive BZ and under X-ray polarization.

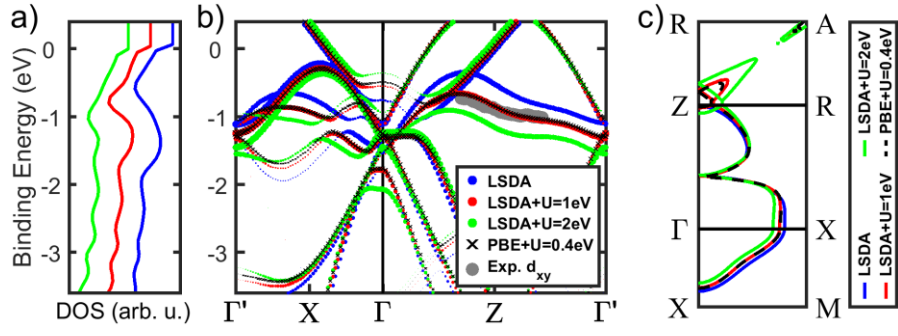


Fig. 3: DFT+ U calculations under variation of U_{eff} : (a) DOS; (b) Unfolded bands along the Γ' -X- Γ -Z- Γ' directions (majority spin only); (c) Corresponding FS. The best match to our ARPES data is achieved with $U_{\text{eff}} = 1$ eV for the LSDA and 0.4 eV for the GGA exchange-correlation (PBE).